

THERMAL OPTIMIZATION RESEARCH OF OIL-IMMERSED TRANSFORMER WINDING BASED ON THE SUPPORT VECTOR MACHINE RESPONSE SURFACE

by

***Fa Ting YUAN^{a,b}, Wen Tao YANG^a, Bo TANG^a, Yue WANG^a, Fa JIANG^a,
Yi Lin HAN^a, Li HUANG^{a*}, and Can DING^a***

^a College of Electrical Engineering and New Energy,
China Three Gorges University, Yichang, China

^b Hubei Provincial Engineering Technology Research Center for Power Transmission-Line,
China Three Gorges University, Yichang, China

Original scientific paper
<https://doi.org/10.2298/TSCI210530264Y>

In this paper, the CFD model is established for the low voltage winding region of an oil-immersed transformer according to the design parameters, and the detailed temperature distribution within the region is obtained by numerical simulation. On this basis, the response surface methodology is adopted to optimize the structure parameters with the purpose of minimizing the hot spot temperature. After a sequence of designed experiments, the second-order polynomial response surface and the support vector machine response surface are established, respectively. The analysis of their errors shows that the support vector machine response surface can be better used to fit the approximation. Finally, the particle swarm optimization algorithm is employed to get the optimal structure parameters of the winding based on the support vector machine response surface. The results show that the optimization method can significantly reduce the hot spot temperature of the winding, which provides a guiding direction for the optimal design of the winding structure of transformers.

Key words: *response surface methodology, winding structure optimization, support vector machine, oil-immersed transformer, hot spot temperature*

Introduction

Since the power transformer is a key component of the power transmission and distribution network, its operation reliability is related to the security and stability of the power grid. When it comes to a transformer, its functioning and life expectancy are dictated mainly by the maximum temperature (*i.e.* the hot spot temperature) of the winding. As the most critical factor affecting the insulation lifetime of the winding, the hot spot temperature meets the typical 6 °C rule in its relationship with the insulation lifetime. Within the temperature ranging from 80-140 °C, the aging rate is doubled and the lifetime is halved with every rise of 6 °C in the winding temperature [1, 2]. Therefore, the optimization of the winding structure based on the accurate prediction of the winding hot spot temperature can effectively improve the working performance of the transformer and prolong its service life.

* Corresponding author, e-mail: huanglictgu@163.com

Previous researches aiming to improve the temperature distribution in the transformer winding and reduce the hot spot temperature can be summarized from the following aspects:

- Before accurately predicting the temperature and the position of the hot spot in the winding, it is necessary to establish a fluid-temperature field coupling model for precise calculation. In this process, thermal hydraulic networks (THN) [3-6] and CFD [7-11] are usually used to describe the entire oil circuit. Compared with the THN, the CFD method provides higher accuracy in predicting temperature distribution and fluid behavior.
- A number of scholars have conducted many comprehensive researches on the influencing factors of the hot spot. For instance, Skillen *et al.* [7] applied CFD software to obtain the temperature distribution and the position of the winding hot spot. It has been found that the hot spot has obvious impact on oil flow. Torriano *et al.* [9] examined the effect of the numerical model, the mass-flow rate and the inlet boundary conditions on the flow and temperature distribution in the transformer winding. Li *et al.* [12] studied the oil flow velocity and the temperature distribution characteristics of a disc-type oil-immersed power transformer, and also analyzed the influence of the inlet oil flow velocity, the width of the horizontal oil channel, the number of winding sections and the conductor turn-to-turn insulation thickness. In addition, the width of the flow cooling channel, the size of the winding, the structure of the transformer and the number and width of block washers have also been verified to produce significant impacts on the hot spot temperature [3, 10, 11, 13]. Although some suggestions are given in these studies on how to improve the temperature distribution in the winding, there is still no specific best optimization design for the winding structure.
- Many optimization studies have been carried out to improve the structure parameters and the working performance of electrical devices. For example, to improve the efficiency of a generator, the numerical simulation and the response surface methodology (RSM) are combined to optimize the stator slot structure of the alternator [14]. The CFD and the genetic algorithm are adopted to optimize the mutual configuration of the winding and cooling channel, resulting in dramatic decrease in the hot spot temperature of the dry-type transformer [15]. The temperature distribution is obtained based on the design parameters of the dry-type reactor, and the amount of metal conductors in the coil is optimized by particle swarm optimization (PSO), thus verifying the correctness of the optimization method [16]. In addition, the orthogonal test method is also applied in combination with numerical simulation to optimize the structure of dry-type air core reactors [17, 18].

In this paper, the finite element method, the RSM, the support vector machine (SVM) and the PSO algorithm are integrated in the optimization of the winding structure of an oil-immersed transformer. The use of this optimization portfolio to optimize the transformer design is absent in the existing studies. The temperature distribution results obtained herein demonstrate sharp reduction in the hot spot temperature of the winding that has the optimized parameters.

Basic structure and equivalent model of the transformer

Basic structure of the transformer winding

Figure 1 shows the structure of the core and the low voltage winding of the transformer. It can be seen that the winding discs made of insulated wires are arranged along the periphery of the core. In the winding region, two vertical (axial) oil channels and several horizontal (radial) oil channels separate the discs and form the channels for the cooling oil flow. At the same time, a block washer is staggered every certain number of discs to force the oil flow to enter into one vertical oil channel and exist from the vertical oil channel on the other side. The

oil flow between each two block washers forms a cooling pass. In this study, five block washers divide the oil flow area into six passes. The cooling of the transformer winding is achieved by the oil flow passing through these passes.

Equivalent model of the transformer winding

In consideration of the little difference between the results of the 2-D and the 3-D model [6, 7], a 2-D axisymmetric approximation model is employed herein to simplify the winding model. Although there are a huge number of heat transfer processes in other regions of the transformer, their impact on the winding region can be ignored [9] (because the thermal conductivity of the cylinder is small, it can be assumed that the heat transfer between the winding region and other areas in the transformer can be ignored).

This paper focuses on the study of the low voltage winding of an oil-immersed transformer (20 MVA, 35/10.5 kV), of which the 2-D model is given in fig. 2. There are 48 discs in the winding region, with each disc composed of six turns of coils, and each turn of coil made of four strands of wires. The cross-section size of the copper conductor is 12.1 mm × 2.0 mm ($H_d \times W_d$) in size, and the outer layer of each conductor is wrapped with 0.4 mm insulating paper. The inlet width and the outlet width of the cooling oil flow are both 8.0 mm. The winding region is divided by five block washers into six passes, and there are eight discs in each pass. The length and the thickness of block washers on both sides are 75.0 mm and 1.0 mm, respectively. All passes are numbered from 1-6 from bottom to top, and the discs in each pass are also numbered from 1-8 from bottom to top. Besides, there are two inner and outer vertical cooling channels with the width of 7.2 mm and 8.0 mm and ten horizontal channels with the width of 4.2 mm in each pass. The detailed geometric parameters are marked in fig. 2.

Numerical simulation of winding temperature field

Governing equations

The heat transfer process of transformer winding region is mainly heat conduction and heat convection [10], and the heat conduction can be shown [19]:

$$\frac{\partial^2 T}{\partial r^2} + \frac{\partial^2 T}{\partial z^2} + \frac{q}{k} = 0 \tag{1}$$

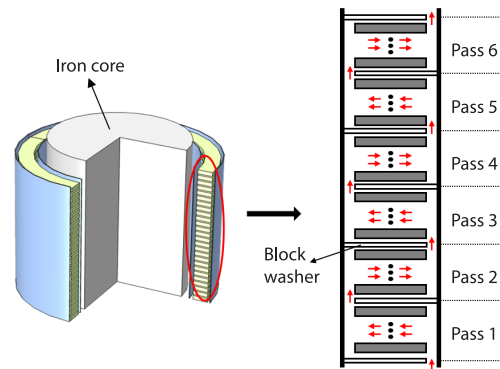


Figure 1. Low voltage winding structure of the transformer

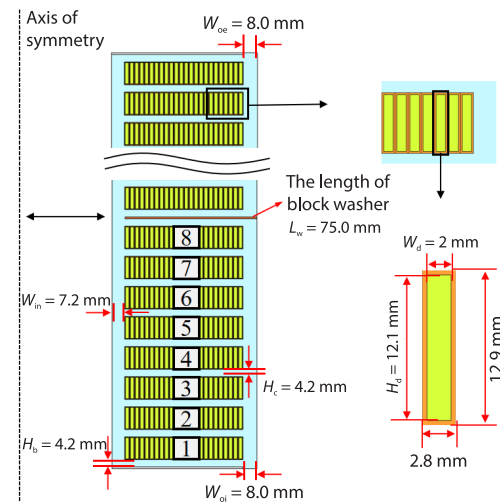


Figure 2. The 2-D axisymmetric model of the low voltage winding

where r and z are the radial and axial co-ordinates of the model, T – the temperature, k – the thermal conductivity, and q – the heat source of conductor. The heat convection between conductors and cooling oil satisfies the conservation of mass, momentum and energy:

$$\begin{aligned} \frac{1}{r} \frac{\partial(ur)}{\partial r} + \frac{1}{z} \frac{\partial(vr)}{\partial z} &= 0 \\ \rho_{\text{oil}} \left(u \frac{\partial u}{\partial r} + v \frac{\partial u}{\partial z} \right) &= F_r - \frac{\partial p}{\partial r} + \mu_s \left(\frac{\partial^2 u}{\partial r^2} + \frac{\partial^2 u}{\partial z^2} \right) \\ \rho_{\text{oil}} \left(u \frac{\partial v}{\partial r} + v \frac{\partial v}{\partial z} \right) &= F_z - \frac{\partial p}{\partial z} + \mu_s \left(\frac{\partial^2 v}{\partial r^2} + \frac{\partial^2 v}{\partial z^2} \right) \\ u \frac{\partial T}{\partial r} + v \frac{\partial T}{\partial z} &= \frac{k_{\text{oil}}}{\rho_{\text{oil}} c_p} \left(\frac{\partial^2 T}{\partial r^2} + \frac{\partial^2 T}{\partial z^2} \right) \end{aligned} \quad (2)$$

where u and v are the radial and axial velocity of the fluid, respectively, ρ_{oil} – the density of the fluid, F_r, F_z are the radial and axial components of body force, respectively, p – the pressure of the fluid, μ_s – the viscosity of the fluid, c_p – the constant pressure specific heat capacity of the fluid, and k_{oil} – the thermal conductivity of the fluid.

Materials properties and boundary conditions

The setting of materials properties is essential for the numerical simulation of the winding. Specifically, the materials properties of the conductor, the insulation paper and the cooling oil are given in tab. 1.

Table 1. Materials properties

Materials	Properties	Value
Conductor (Cu)	Density [kgm^{-3}]	8933
	Specific heat [$\text{Wkg}^{-1}\text{K}^{-1}$]	385
	Thermal conductivity [$\text{Wm}^{-1}\text{K}^{-1}$]	401
Insulation paper	Density [kgm^{-3}]	930
	Specific heat [$\text{Wkg}^{-1}\text{K}^{-1}$]	1340
	Thermal conductivity [$\text{Wm}^{-1}\text{K}^{-1}$]	0.19
Cooling oil	Density [kgm^{-3}]	$1098.72 - 0.712T$
	Specific heat [$\text{Wkg}^{-1}\text{K}^{-1}$]	$807.163 + 3.58T$
	Thermal conductivity [$\text{Wm}^{-1}\text{K}^{-1}$]	$0.1509 - 7.1 \cdot 10^{-5}T$
	Viscosity [$\text{kgm}^{-1}\text{s}^{-1}$]	$0.08467 - 4 \cdot 10^{-4}T + 5 \cdot 10^{-1}T^2$

According to the geometric characteristics and materials properties of the transformer winding, the boundary conditions for the model are set at the inlet of Pass 1, the oil flow moves at the uniform velocity of 0.05 m/s and the temperature of 313 K. The pressure at the outlet of the cooling pass is set as 0 Pa. In addition, given the negligible thermal conductivity of the inner and outer walls of the winding and block washers, these parts are set as the adiabatic boundaries and the heat exchange among them is not considered. Each conductor is assumed to have uniform loss in the heat source and have the power of 52.47 W. Since each disc consists of 24 conductors, the total heating power of each disc is 1259.28 W.

Simulation results

The temperature field simulation results of winding can be obtained according to heat source loading, the setting of materials properties and boundary conditions, as shown in fig. 3.

In fig. 3, the temperature in each pass basically shows an upward trend with the increase of the height in the axial direction, and the hot spot is located in the middle discs. In the radial direction, despite the opposite directions of the oil flow in any two connected passes due to the staggered setting of the block washers, it can be observed that the temperature on each disc always rises along the oil flow direction until approaching the vertical channel on the other side. Furthermore, the maximum velocity of the oil flow in each horizontal channel extracted along the radial perpendicular bisector of the winding is shown in fig. 4. The velocity of the oil flow is constantly positive regardless of the oil flow direction.

In order to get more detailed and intuitive temperature distribution in the winding and obtain the relationship between heat transfer and fluid-flow, the maximum temperatures on each disc are extracted and shown in fig. 5.

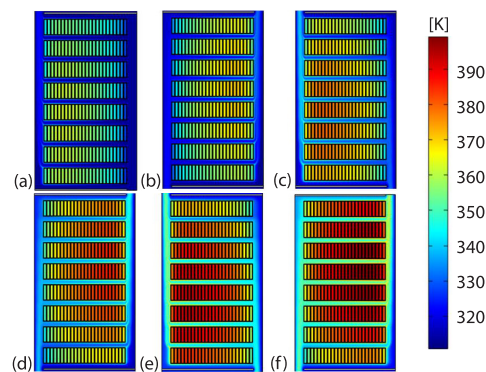


Figure 3. Temperature distribution of the winding; (a) Pass 1, (b) Pass 2, (c) Pass 3, (d) Pass 4, (e) Pass 5, and (f) Pass 6

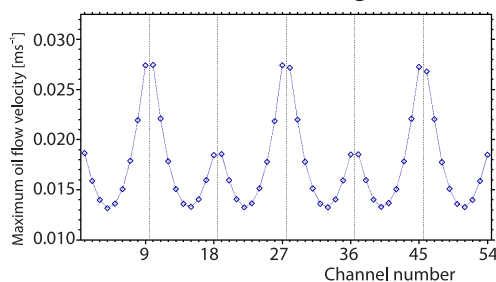


Figure 4. Maximum velocity of the oil flow in each channel

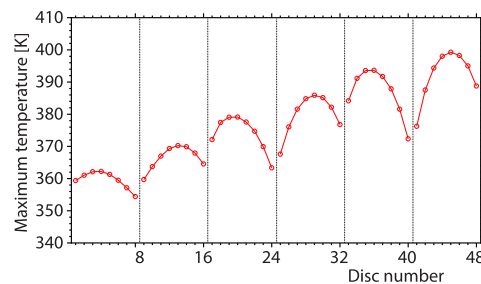


Figure 5. Maximum temperature on each disc

As shown in figs. 4 and 5, the maximum velocity of the oil flow and the maximum temperature on each disc are periodically distributed, and there are higher oil flow velocity and lower temperature on both sides of each block washer. There is a negative correlation between the temperature on each disc and the flow velocity in the horizontal channels on both sides of the disc, which can be explained that the influences of heat convection will be enlarged by the higher velocity.

Grid testing

The grid testing is carried out to guarantee mesh-independent solutions. In all CFD simulations, the meshes consist of layers of thin rectangles for the flow boundary-layers and triangles for other places. The element size close to the walls is quite small in order to well capture the temperature and velocity gradients. The tracking parameters at each number of elements are the hot spot temperature, T_{hs} , and the maximum flow velocity, V_{max} , as shown in tab. 2. It can be deduced that the T_{hs} and V_{max} reach a stable value when the elements number is 598420. The T_{hs} of 399.25 K will be used as the benchmark for the subsequent optimization.

Table 2. Grid testing results

Number of elements	275715	424371	514876	598420	929855
T_{hs} [K]	398.67	399.13	399.24	399.25	399.27
V_{max} [mms ⁻¹]	94.61	96.82	97.92	98.11	98.20

Optimization design of the winding structure

In the engineering optimization design, the application of the RSM can greatly reduce the time required for experiment or numerical calculation. The response surface refers to the relationship between responses and design variables. The basic idea of the RSM [20] is to use a sequence of designed experiments at the first stage. At present, central composite design (CCD) is one of the most classic and widely used designs, consequently the CCD is used in this paper. In the second stage, by using these experimental results, the second-order regression modelling is performed to establish the non-linear relations between the design variables and responses. Moreover, an optimization algorithm is adopted to approximate the optimal solution. In this study, the RSM is applied to optimize the winding structure, with the hot spot temperature as the response and the structure parameters as the design variables.

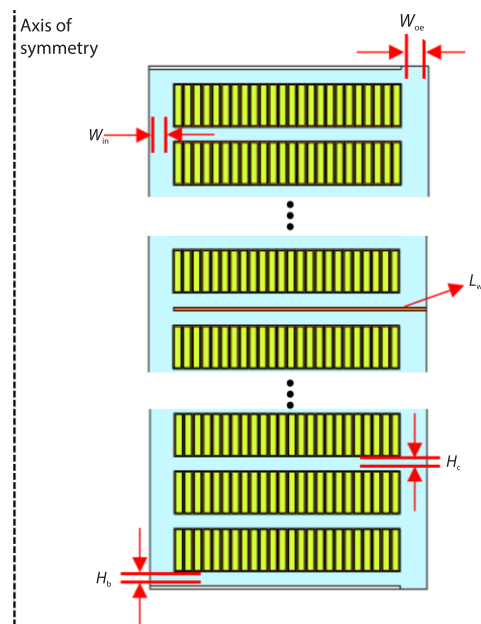


Figure 6. Design variables of winding structure

The CCD of winding structure parameters

According to the structural characteristics of the low voltage winding, the five parameters which mainly influence the hot spot temperature are selected: the width of the inner vertical oil channel, W_{in} , the width of the bottom horizontal oil channel, H_b , the width of the horizontal oil channel between discs, H_c , the length of the block washer, L_w , and the width of the oil flow outlet, W_{oc} , as shown in fig. 6.

In the CCD experiment, the hot spot temperature, T_{hs} , of each sample is obtained by the numerical simulation established in section *Numerical simulation of winding temperature field*. Except the five selected parameters that are set according to the experimental design table, the parameters of the disc and other winding components remain unchanged. Table 3 shows the design table with the five factors and five levels obtained according to the standard of CCD. A total of 50 samples are conducted, among which seven samples are repeated.

Establishment of the response surfaces

The second-order polynomial response surface and the SVM response surface model are established, respectively according to the results given in tab. 3.

Table 3. The CCD experimental design

Sample	W_{in} [mm]	H_b [mm]	H_c [mm]	L_w [mm]	W_{oc} [mm]	T_{hs} [K]
1	8.00	4.20	4.00	77.00	6.00	399.37
2	6.40	4.20	4.40	73.00	10.00	402.65
3	8.00	4.20	4.40	77.00	10.00	393.17
4	8.00	3.20	4.00	73.00	6.00	402.70
5	7.20	3.70	3.72	75.00	8.00	406.03
6	7.20	3.70	4.20	75.00	3.24	399.42
7	6.40	4.20	4.00	73.00	6.00	410.95
8	7.20	3.70	4.20	75.00	8.00	399.15
9	6.40	3.20	4.40	73.00	6.00	401.95
10	6.40	3.20	4.40	77.00	6.00	400.81
11	8.00	4.20	4.40	77.00	6.00	393.17
12	6.40	3.20	4.00	73.00	10.00	408.94
13	7.20	3.70	4.20	75.00	12.76	399.45
14	7.20	3.70	4.20	79.76	8.00	390.79
15	6.40	4.20	4.40	73.00	6.00	403.05
16	8.00	4.20	4.40	73.00	10.00	395.06
17	7.20	3.70	4.68	75.00	8.00	412.54
18	5.30	3.70	4.20	75.00	8.00	423.39
19	6.40	4.20	4.00	73.00	10.00	411.05
20	8.00	4.20	4.40	73.00	6.00	394.96
21	6.40	3.20	4.40	77.00	10.00	400.52
22	9.10	3.70	4.20	75.00	8.00	401.98
23	8.00	3.20	4.40	77.00	10.00	392.64
24	7.20	4.89	4.20	75.00	8.00	399.43
25	6.40	4.20	4.00	77.00	6.00	403.90
26	8.00	3.20	4.40	73.00	6.00	394.20
27	8.00	3.20	4.00	77.00	10.00	397.97
28	7.20	3.70	4.20	75.00	8.00	399.15
29	8.00	3.20	4.40	73.00	10.00	394.26
30	6.40	4.20	4.00	77.00	10.00	404.20
31	6.40	4.20	4.40	77.00	10.00	402.21
32	8.00	4.20	4.00	77.00	10.00	399.63
33	7.20	3.70	4.20	75.00	8.00	399.15
34	6.40	3.20	4.00	73.00	6.00	408.92
35	7.20	2.51	4.20	75.00	8.00	399.72
36	8.00	4.20	4.00	73.00	10.00	406.39
37	7.20	3.70	4.20	75.00	8.00	399.15
38	8.00	3.20	4.40	77.00	6.00	392.69
39	6.40	4.20	4.40	77.00	6.00	402.69
40	7.20	3.70	4.20	75.00	8.00	399.15
41	7.20	3.70	4.20	70.24	8.00	400.93
42	8.00	4.20	4.00	73.00	6.00	406.00
43	6.40	3.20	4.40	73.00	10.00	401.70
44	6.40	3.20	4.00	77.00	6.00	403.20
45	8.00	3.20	4.00	73.00	10.00	402.99
46	7.20	3.70	4.20	75.00	8.00	399.15
47	6.40	3.20	4.00	77.00	10.00	403.38
48	7.20	3.70	4.20	75.00	8.00	399.15
49	8.00	3.20	4.00	77.00	6.00	397.83
50	7.20	3.70	4.20	75.00	8.00	399.15

Second-order polynomial response surface

The response surface mathematical model used in the RSM is usually a second-order polynomial equation, which is calculated from the data obtained from the experimental design by least square method:

$$Y = \beta_0 + \sum_{i=1}^k \beta_i X_i + \sum_{i=1}^k \beta_{ii} X_i^2 + \sum_{\substack{i=1 \\ i < j}}^k \beta_{ij} X_i X_j \quad (3)$$

where Y is the corresponding response, X_i – the value of the input parameter, k – the number of variables, $\beta_0, \beta_i, \beta_{ii}$ and β_{ij} are the regression coefficients, which are estimated by a regression from a set of observations of the response, i and j – the linear and quadratic coefficients, respectively.

According to the structure parameters and the corresponding T_{hs} in tab. 3, the following second-order polynomial response surface is fitted:

$$\begin{aligned} T_{hs} = & 983.2711 - 32.05827W_{in} + 26.28467H_b - 522.64727H_c + 17.20106L_w + 1.49534W_{oc} + \\ & + 0.092969W_{in}H_b - 4.64258W_{in}H_c - 0.039258W_{in}L_w - 2.30313H_bH_c - 0.16094H_bL_w + \\ & + 0.00531H_bW_{oc} + 3.01016H_cL_w - 0.23359H_cW_{oc} - 0.00195L_wW_{oc} + 3.40007W_{in}^2 - \\ & - 0.56599H_b^2 + 39.37512H_c^2 - 0.19956L_w^2 - 0.04156W_{oc}^2 \end{aligned} \quad (4)$$

where the second-order polynomial response surface reflecting the relationship between the winding structure parameters and the hot spot temperature is established.

The SVM response surface

Support vector machine

The SVM is a modelling method based on small sample statistical learning theory and structural risk minimization [21, 22]. The training sample S can be represented:

$$S = \{(x_1, y_1), \dots, (x_n, y_n)\} \subset R^n \times R \quad (5)$$

where x_i is the i^{th} input vector, y_i – the corresponding output vector, and n – the number of samples. The SVM maps the sample x in the input space to the high dimensional feature space H by the non-linear mapping function $\varphi(x)$, and the linear regression function in H is established by using the principle of structural risk minimization:

$$y' = w\varphi(x) + b \quad (6)$$

where y' is the predicted value, y – the measured value, $w \in H$ and is the weight vector, $b \in R$ and is the offset. The problem of regression fitting can be solved by introducing the ε -insensitive loss function based on SVM. The relaxation factor ξ_i and ξ_i^* are introduced, and with the principle of structural risk minimization, the regression problem is transformed into the problem of minimizing the objective function of structural risk, which means to find the values of w and b to minimize the objective function:

$$\begin{aligned} \min \left\{ \varphi(w) = \frac{1}{2} \|w\|^2 + C \sum_{i=1}^n (\xi_i + \xi_i^*) \right\} \\ \text{s.t.} \begin{cases} w\varphi(x_i) - y_i + b \leq \varepsilon + \xi_i^* \\ y_i - w\varphi(x_i) - b \leq \varepsilon + \xi_i \\ \xi_i \geq 0, \xi_i^* \geq 0 \end{cases} \end{aligned} \quad (7)$$

where the constant C is the penalty factor and the value of $C > 0$.

When solving eq. (7), a non-negative Lagrange multiplier to construct Lagrange function is introduced, and the problem is transformed into solving the saddle point of Lagrange equation. The partial derivatives of each variable in the equation are calculated and made zero, respectively. By using the duality principle, it is transformed into solving the dual problem:

$$\begin{aligned} \max & \left\{ -\frac{1}{2} \sum_{i,j=1}^n (\alpha_i - \alpha_i^*)(\alpha_j - \alpha_j^*)K(x_i, x_j) - \varepsilon \sum_{i=1}^n (\alpha_i + \alpha_i^*) + \sum_{i=1}^n y_i (\alpha_i - \alpha_i^*) \right\} \\ \text{s.t.} & \sum_{i=1}^n (\alpha_i - \alpha_i^*) = 0 \quad \alpha_i, \alpha_i^* \in [0, C] \end{aligned} \quad (8)$$

where $K(x_i, x_j) = \varphi(x_i)^T \varphi(x_j)$ is the kernel function. Different kernel functions correspond to different SVM. The radial basis function (RBF) has the characters of simple parameters and can effectively realize non-linear mapping. Therefore, RBF kernel function is used in this paper:

$$K(x_i, x_j) = \exp(-\gamma \|x_i - x_j\|^2) \quad (9)$$

where γ is the kernel parameter and greater than zero. The optimal hyperplane expression of the corresponding training:

$$y' = \sum_{i=1}^n (\alpha_i - \alpha_i^*)K(x_i, x_j) + b \quad (10)$$

The LIBSVM toolbox developed by Dr. Lin Zhiren of Taiwan University is used to solve the problem of the SVM.

Establishment of SVM response surface

Considering the different dimensions of transformer winding structure parameters, it is necessary to normalize the data to eliminate the influence of different orders of magnitude. These features are normalized by:

$$x'_i = \frac{x_i - x_{\min}}{x_{\max} - x_{\min}} \quad (11)$$

where x'_i is the normalized value of a parameter, x_i – the actual value of the parameter, and x_{\max} , x_{\min} are the maximum and minimum values of the parameter in all samples, respectively.

The optimal values of penalty coefficient, C , and kernel function parameter, γ , are searched based on the idea of K -fold cross-validation. The original data is divided into K groups, among which $K-1$ groups are regarded as training samples and the remaining one group is used as the test sample for each testing. According to the CCD experimental design in tab. 3, the original data are divided into ten groups, of which nine groups are regarded as training samples, and the remaining one group is used as test sample for each test. The parameters of grid search are set the range of penalty parameter, C , is $[2^{-10}, 2^{20}]$, and the step size is 2. The range of nuclear parameter, γ , is $[2^{-10}, 2^{20}]$, and the step size is 2. Finally, the results of C and γ are obtained by grid search, as shown in tab. 4.

Table 4. The optimal values of penalty coefficient and kernel function parameter

Parameter	Optimal value
C	2.0
γ	1.0

Error analysis

The advantages and disadvantages of response surfaces can be evaluated scientifically by the error analysis. In order to evaluate the prediction ability of response surfaces comprehensively, and without too much time to test and verify, it is necessary to select a representative combination test results as a reference. The orthogonal test design is another design of experiment to study multi factors and multi-level [23], which is to select some representative points from comprehensive tests and these points have the characteristics of dispersion, uniformity and comparability. Therefore, the orthogonal experimental results are used as test sets to compare the accuracy of two response surfaces. Targeting at the inner vertical oil channel width, W_{in} , the bottom horizontal oil channel width, H_b , the horizontal oil channel width, H_c , the block washer length, L_w , and the oil flow outlet width, W_{oc} , the $L_{16}(4^5)$ orthogonal test with five factors and four levels is obtained as shown in tab. 5.

Table 5. Orthogonal experiment table

Sample	W_{in} [mm]	H_b [mm]	H_c [mm]	L_w [mm]	W_{oc} [mm]
1	6.00	2.95	4.05	72.00	5.00
2	6.00	3.45	4.15	74.00	7.00
3	6.00	3.95	4.25	76.00	9.00
4	6.00	4.45	4.35	78.00	11.00
5	6.80	2.95	4.15	76.00	11.00
6	6.80	3.45	4.05	78.00	9.00
7	6.80	3.95	4.35	72.00	7.00
8	6.80	4.45	4.25	74.00	5.00
9	7.60	2.95	4.25	78.00	7.00
10	7.60	3.45	4.35	76.00	5.00
11	7.60	3.95	4.05	74.00	11.00
12	7.60	4.45	4.15	72.00	9.00
13	8.40	2.95	4.35	74.00	9.00
14	8.40	3.45	4.25	72.00	11.00
15	8.40	3.95	4.15	78.00	5.00
16	8.40	4.45	4.05	76.00	7.00

According to the parameters in the aforementioned samples, the second-order polynomial response surface and SVM response surface are used to predict the T_{hs} , and the values obtained by the two methods are compared with the numerical simulation results. The difference ΔT_{hs} can be shown:

$$\Delta T_{hs,i} = T_{hs,i} - T'_{hs,i} \quad (12)$$

where $T_{hs,i}$ and $T'_{hs,i}$ are the T_{hs} of the i^{th} sample predicted by numerical simulation and response surfaces, respectively. The results are shown in fig. 7.

In fig. 7, it can be concluded that the difference between the T_{hs} predicted by the two response surfaces and the numerical simulation results is small. In this paper, the root mean squared error (RMSE) is also used to compare the predicted and numerical simulation results, namely:

$$RMSE = \sqrt{\frac{1}{N} \sum_{i=1}^N (T_{hs,i} - T'_{hs,i})^2} \quad (13)$$

Comparing the RMSE of 16 samples, the RMSE of the second-order polynomial response surface is 1.92, while of the SVM response surface is 1.71. Although there is still a certain gap between the results of the two response surfaces and of the numerical simulation, the T_{hs} with different structure parameters can be well predicted. Compared with the second-order polynomial response surface, the RMSE of T_{hs} predicted by SVM response surface is less than 10.93%, which proves its feasibility and effectiveness. Thus, the SVM response surface obtained in this section is the basis of the optimization in the following study.

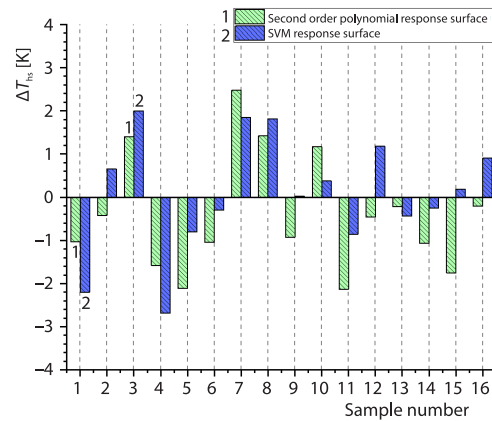


Figure 7. The ΔT_{hs} of 16 samples

The optimization result based on the SVM response surface

The PSO [24] is an effective multi parameter optimization algorithm. When PSO is used to solve the optimization problem, it corresponds to searching the position of a particle in the space. Each particle has its own position and velocity (which determines the direction and distance of motion), and a fitness value determined by the optimization functions. Each particle memorizes the current optimal particle, and then searches the best position in the solution space. The process of each iteration is not completely random. If a better solution is obtained, the next solution will be found based on it. Since PSO is rather simple and easy to implement, fast to solve problems, and there are not many parameters to be adjusted, the PSO algorithm is selected to optimize the winding structure based on the SVM response surface.

In the optimization process of PSO, the parameters are set the acceleration factors c_1 and c_2 are both 1.5. The inertia weight w is 0.8 and the number of particles n is 100. The number of iterations K is 1000. The objective of the optimization is to minimize the hot spot temperature, and the constraint equations are:

$$\begin{aligned} 5.30 &\leq W_{in} \leq 9.10 \\ 2.51 &\leq H_b \leq 4.89 \\ 3.72 &\leq H_c \leq 4.68 \\ 70.24 &\leq L_w \leq 79.76 \\ 3.24 &\leq W_{oc} \leq 12.96 \end{aligned} \quad (14)$$

Combined with the SVM response surface and the PSO algorithm, the lowest winding hot spot temperature is 389.45 K, and the five structure parameters at this temperature are as shown in tab. 6.

Table 6. The winding structure parameters before and after optimization

Parameter	W_{in} [mm]	H_b [mm]	H_c [mm]	L_w [mm]	W_{oc} [mm]
Before optimization	7.20	4.20	4.20	75.00	8.00
After optimization	7.85	3.50	4.32	79.76	8.09

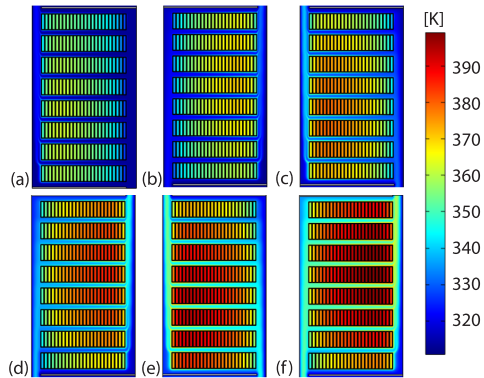


Figure 8. Temperature distribution of low voltage winding with the optimal parameters, (a) Pass 1, (b) Pass 2, (c) Pass 3, (d) Pass 4, (e) Pass 5, and (f) Pass 6

The temperature distribution of each pass can be obtained by numerical simulation based on the optimal winding structure, as shown in fig. 8. Besides, the maximum temperatures on each disc before and after optimization are extracted and shown in fig. 9.

It can be obtained that the T_{hs} of winding is 389.99 K, which is 9.26 K lower than that of the original model. Besides, fig. 9 shows that the temperature distribution in each pass has been improved obviously after optimization. Thus, the feasibility and effectiveness of the optimization method is proved.

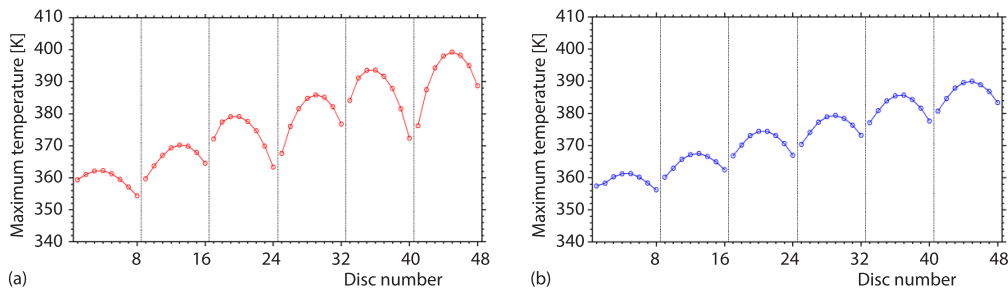


Figure 9. Maximum temperature on each disc before and after optimization; (a) before optimization and (b) after optimization

Conclusions

In this paper, the low voltage winding of a transformer is modeled on the COMSOL simulation platform, and the winding structure parameters are optimized to reduce the hot spot temperature. The conclusions can be achieved as follows.

- The temperature distribution of the low voltage winding region is obtained by numerical simulation, and there is a higher temperature on the discs in the top pass. In addition, the distribution of oil flow velocity in channels and the maximum temperature on each disc shows the characteristic of periodic distribution, and there is a negative correlation between the temperature on the disc and the oil flow velocity on both sides of discs.
- The non-linear relationship between winding structure parameters and the hot spot temperature is established according to the CCD table by numerical simulation, and the second-order polynomial response surface and the SVM response surface are constructed, respectively. Compared with the former response surface, the RMSE between the prediction results of the SVM response surface and the numerical simulation is 10.93% smaller, which proves its accuracy and better approximation to the actual response surface.
- The response surface which reflects the relationship between the winding structure parameters and the hot spot temperature can be optimized quickly and accurately. In this case, the hot spot temperature of the winding is reduced by 9.25 K adopting the PSO based on

the SVM response surface, which effectively improves the working performance of the transformer. Meanwhile, the 3-D simulation model of the transformer can be established in the future research, and the optimization of the whole winding structure can be realized by referring to the previous method.

Acknowledgment

This work was supported by Hubei Provincial Natural Science Foundation of China (No. 2020CFB376), Yichang Science and Technology Project (No. A21-3-010), Open Fund of State Key Laboratory of Power Grid Environmental Protection (No. GYW51202101368).

Nomenclature

c_p – specific heat capacity of the fluid, [Wkg ⁻¹ K ⁻¹]	T – temperature, [K]
F_r – radial components of body force, [N]	T_{hs} – hot spot temperature, [K]
F_z – axial components of body force, [N]	u – radial velocity of the fluid, [ms ⁻¹]
H_b – width of the bottom horizontal oil channel, [mm]	V_{max} – maximum flow velocity, [mms ⁻¹]
H_c – width of the horizontal oil channel between discs, [mm]	v – axial velocity of the fluid, [ms ⁻¹]
k – thermal conductivity, [Wm ⁻¹ K ⁻¹]	W_{in} – width of the inner vertical oil channel, [mm]
k_{oil} – thermal conductivity of the fluid, [Wm ⁻¹ K ⁻¹]	W_{oc} – width of the oil flow outlet, [mm]
L_w – length of the block washer, [mm]	W_{oi} – width of the oil flow inlet, [mm]
p – pressure of the fluid, [Pa]	z – axial co-ordinate of the model, [mm]
q – power of the heat source, [Wm ⁻³]	
r – radial co-ordinates of the model, [mm]	

Greek symbols

μ_s – viscosity of the fluid, [kgm ⁻¹ s ⁻¹]
ρ_{oil} – density of the fluid, [kgm ⁻³]

Reference

- [1] ***, Loading Guide for Oil-immersed Power Transformers, *IEC. Standard 60076-7*, 2018
- [2] ***, Guide for Loading Mineral-oil-immersed Transformers, *IEEE. Standard C57.91*, 2011
- [3] Rahimpour, E., *et al.*, An Investigation of Parameters Affecting the Temperature Rise in Windings with Zigzag Cooling Flow Path, *Applied Thermal Engineering*, 27 (2007), 11, pp. 1923-1930
- [4] Zhang, J., Li X., Oil Cooling for Disk-Type Transformer Windings – Part 1: Theory and Model Development, *IEEE Transactions on Power Delivery*, 21 (2006), 3, pp. 1318-1325
- [5] Radakovic, Z. R., Sorgic, M. S., Basics of Detailed Thermal-Hydraulic Model for Thermal Design of Oil Power Transformers, *IEEE Transaction on Power Delivery*, 25 (2010), 2, pp. 790-802
- [6] Codde, J., *et al.*, Assessment of a Hydraulic Network Model for Zig-Zag Cooled Power Transformer Windings, *Applied Thermal Engineering*, 80 (2015), Apr., pp. 220-228
- [7] Skillen, A., *et al.*, Numerical Prediction of Local Hot-Spot Phenomena in Transformer Windings, *Applied Thermal Engineering*, 36 (2012), Apr., pp. 96-105
- [8] Campelo, H. M. R., *et al.*, Numerical Thermofluid Analysis of a Power Transformer Disc-Type Winding, *Proceedings*, 2016 IEEE Electrical Insulation Conference (EIC), Montreal, Canada, 2016, pp. 21-28
- [9] Torriano, F., *et al.*, Numerical Study of Parameters Affecting the Temperature Distribution in a Disc-Type Transformer Winding, *Applied Thermal Engineering*, 30 (2010), 14-15, pp. 2034-2044
- [10] Zhang, X., *et al.*, Numerical Investigation of Oil Flow and Temperature Distributions for ON Transformer Windings, *Applied Thermal Engineering*, 130 (2018), Feb., pp. 1-9
- [11] Zhang, X., *et al.*, Prediction of Pressure Drop and Flow Distribution in Disc-type Transformer Windings in an OD Cooling Mode, *IEEE Transactions on Power Delivery*, 32 (2016), 4, pp. 1655-1664
- [12] Li, L., *et al.*, Analysis of Influence Factors on Temperature Rise of Disc-type Winding of Oil Immersed Power Transformer (in Chinese), *Electric Power Automation Equipment*, 36 (2016), 12, pp. 83-88
- [13] Wakil, N. E., *et al.*, Numerical Study of Heat Transfer and Fluid-flow in a Power Transformer, *International Journal of Thermal Sciences*, 36 (2016), 12, pp. 83-88
- [14] Karaoglan, A. D., *et al.*, Design Optimization of Magnetic Flux Distribution for PMG by Using Response Surface Methodology, *IEEE Transactions on Magnetics*, 56 (2020), 6, pp. 1-9
- [15] Smolka, J., *et al.*, The CFD-Based 3-D Optimization of the Mutual Coil Configuration for the Effective Cooling of an Electrical Transformer, *Applied Thermal Engineering*, 50 (2013), 1, pp. 124-133

- [16] Yuan, F., *et al.*, Electromagnetic-Thermal Characteristics Analysis of Dry-type Core Reactor and Optimization Design based on the Particle Swarm Algorithm, *IEEJ Transactions on Electrical and Electronic Engineering*, 16 (2021), 4, pp. 1-9
- [17] Yuan, F., *et al.*, Thermal Optimization for Nature Convection Cooling Performance of Air Core Reactor with the Rain Cover, *IEEJ Transactions on Electrical and Electronic Engineering*, 13 (2018), 2, pp. 1-9
- [18] Yuan, F., *et al.*, The Optimization Design of Sound Arrester for the Dry Type Air Core Smoothing Reactor based on the Multi-physical Field Coupling Method, *IEEJ Transactions on Electrical and Electronic Engineering*, 16 (2021), 5, pp. 704-714
- [19] Yuan, F., *et al.*, Optimization Design of Oil-Immersed Iron Core Reactor based on the Particle Swarm Algorithm and Thermal Network Mode, *Mathematical problems in Engineering*, 2021 (2021), ID6642620
- [20] Deniz, B., Ismail, H. B., Modelling and Optimization I: Usability of Response Surface Methodology, *Journal of food engineering*, 78 (2007), 3, pp. 836-845
- [21] Sain, S. R., The Nature of Statistical Learning Theory, *IEEE Transactions on Neural Networks*, 38 (1997), 4, p. 409
- [22] Zhou, Z., *Machine Learning* (in Chinese), Tsinghua University Press, Beijing, China 2016
- [23] Rao, R. S., *et al.*, The Taguchi Methodology as a Statistical Tool for Biotechnological Applications: A Critical Appraisal, *Biotechnology Journal*, 3 (2008), 4, pp. 510-523
- [24] Eberhart, R., Kennedy, J., A New Optimizer Using Particle Swarm Theory, *Proceedings*, 6th International Symposium on Micro Machine and Human Science, Nagoya, Japan, 1995, pp. 39-43